Multiple-contact discrete-element model for simulating dense granular media

Nicolas Brodu,[1,2] Joshua A. Dijksman,[2,3] and Robert P. Behringer[2]

[1]*INRIA, 200 Avenue de la Vieille Tour, 33405 Talence, France*

[2]*Department of Physics & Center for Nonlinear and Complex Systems, Duke University, P.O. Box 90305, Durham, North Carolina 27708-0305, USA*

[3]*Laboratory of Physical Chemistry and Colloid Science, Wageningen University, P. O. Box 8038, 6700EK Wageningen, The Netherlands*

This article presents a new force model for performing quantitative simulations of dense granular materials. Interactions between multiple contacts (MC) on the same grain are explicitly taken into account. Our readily applicable MC-DEM method retains all the advantages of discrete-element method simulations and does not require the use of costly finite-element methods. The new model closely reproduces our recent experimental measurements, including contact force distributions in full 3D, at all compression levels of the packing up to the experimental maximum limit of 13%. Comparisons with classic simulations using the nondeformable spheres approach, as well as with alternative models for interactions between multiple contacts, are provided. The success of our model, compared to these alternatives, demonstrates that interactions between multiple contacts on each grain must be included for dense granular packings.

I. INTRODUCTION

Dense particulate media such as sand, emulsions, and colloids are ubiquitous in nature and in industry. However, understanding their very rich mechanical behavior has been notoriously difficult. Numerical simulations are an essential tool to access the microscopic and macroscopic behavior of these systems. In principle, the application of solid mechanics and Newton's laws of motion to every grain in a packing should recover that packing's macroscopic behavior. These simulations are typically referred to as discrete-element methods (DEM) [1] and tremendous progress has been made since the classic work of Cundall and Strack [2]. However, getting quantitative agreement between experimental results and DEM simulations is often a challenge. This is partly due to the lack of microscopic structure and force data in experiments on dense particulate media; usually only boundary stresses are available. In the last decade, however, much progress has been made in obtaining microstructural data in two- and three-dimensional model experiments in emulsions [3,4] and granular materials [5–7]. We have recently experimentally measured all grain-scale properties for a 3D granular system, including interparticle contact forces, as the system was subject to controlled strain [8]. These experimental approaches provide a testing ground for DEM models. We show that conventional DEM methods need modification to give a good quantitative match to our recent 3D experimental data.

We propose a method dubbed multicontact DEM (MC-DEM) that significantly improves the predictive power of DEM methods, while retaining their conceptual simplicity. The essential ingredient is that our method computes an overall grain shape deformation induced by particle contacts. This allows for two key effects that are not taken into account in traditional DEM: (i) shape deformations induce the formation of new contacts; (ii) every contact force is affected by other contact forces in its vicinity. We show that our method is in very good agreement with our recent 3D experimental results [8]. Importantly, our method does not involve finite-element method (FEM) calculations. Particle shape deforma-

tions are computed with analytic linear elasticity calculations. More generally, the same method should be applicable to all particulate media where a relation between shape and deformation is readily available, such as for emulsions or foams [9].

II. BACKGROUND

The conventional DEM approach [1] assumes that all contact forces are binary, i.e., independent of forces acting elsewhere on a particle. This is not rigorously true, since the deformation of a particle at a contact generates strain that propagates internally, thereby correlating with deformations at other contacts on the same particle. Due to Newton's third law, these correlations additionally propagate to nearby particles and throughout the whole packing. The binary assumption avoids computational complexity and makes conventional DEM feasible. The main ingredient in our new DEM method is to add interactions between multiple contacts on the same grain, as sketched in Fig. 1, but without incurring long-range effects.

Typically, the normal component of a DEM force law is described in terms of the "overlap," δ of grains, and the resulting force is proportional to $\delta^{3/2}$ for Hertz' law or to δ^1 for linear springs. Depending on the model, various features are added: plasticity, cohesion, tangential forces to account for surface friction, etc. Without correlation between contacts, this method is similar in spirit to a mean-field approach and provides only a first-order description of the granular assembly properties. Hence, a more accurate effective multicontact force model must correct for this, by including the coupling of forces at multiple contacts on a given particle, which is what we do in our model. Of course, for granular gases [10], or loose granular flows [11], binary collisions are a good approximation. The situation is different in dense granular packings near or above jamming. Here, force propagation through long-lasting multiple contacts per particle are the norm and clearly highly relevant for dynamics [12,13].

Usual DEM model
- Independent contacts $F_C = f(\delta_c)$
- Nondeformable spheres

Proposed model
- Multiple contacts $F_C = f(\delta_c, \delta_i, \delta_j, \delta_k, \delta_l)$
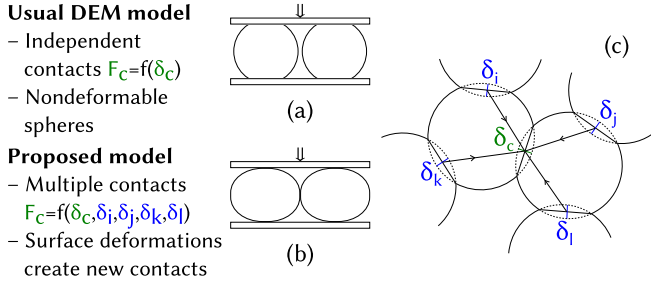- Surface deformations create new contacts

FIG. 1. (Color online) When squeezing a packing of particles, particles deform and new contacts are formed. Traditional DEM (a) does not take this into account. Our multiple contacts model (b) captures these by correcting contact deformation δ_c using linearly additive corrections from other contacts $\delta_{k \to c}$, making (c) the local force depend on all particle contacts $F_c = f(\delta_c, \delta_i, \delta_j, \delta_k, \delta_l)$.

III. INTRODUCING MULTIPLE INTERACTIONS

Interaction schemes for multiple contacts have been proposed [14] but not in the context of DEM. The idea is to model the mutual influence of contacts. This is done by using information on deformations induced by one contact force on the other contacts acting on the grain [Fig. 1(c)] . The displacement fields $\delta_{k \to c}$ in the normal direction, induced by the deformations at other contacts δ_k, are then added to the particle deformation at the local contact δ_c [14], before applying Hertz's law $F \propto (\delta_c + \sum_k \delta_{k \to c})^{3/2}$. At this point, various choices may be made for the form of that displacement field $\delta_{k \to c}$. A first choice is to use the solution for a point force on a sphere [15], which we consider below. A second choice is to consider the stresses induced by an extended surface contact between two spheres [16], which is approximated in a simpler form in Ref. [14]. Unfortunately, while these models may work well for spheres in isolation (i.e., dilute flows, where the contact model matters less), there is no theoretical justification for choosing a solution based on a spherical boundary condition for dense packings, where that boundary may be a very complicated set of free surfaces between contacts. In this work, we therefore simply consider the solution for a point force on an infinite half-space, arguing that the dense packing more closely resembles this situation than that of an isolated sphere. In the quantitative comparisons with experimental data below, we find that our effective infinite half-space approach works better than the other particle-level perspectives. Using the notation of Fig. 2, we express the point force on the elastic half-space solution from [17, 5.4.4] in a vectorial form as

$$\delta_{k \to c} = -\gamma \frac{(1+\nu)F_k}{2\pi E d_{kc}} \Bigg\{ (\mathbf{n}_k \cdot \mathbf{u}_{kc})(\mathbf{n}_c \cdot \mathbf{u}_{kc})$$
$$+ (3 - 4\nu)\mathbf{n}_k \cdot \mathbf{n}_c - (1 - 2\nu)\frac{(\mathbf{n}_k + \mathbf{u}_{kc}) \cdot \mathbf{n}_c}{1 + \mathbf{n}_k \cdot \mathbf{u}_{kc}} \Bigg\}, \quad (1)$$

with F_k the force at contact k, E the Young's modulus of the material, and ν its Poisson's ratio. If the contacts k and c are restricted to be exactly on the surface of a nondeformable sphere, then for $\nu = 0.5$ (and only that case) the half-space solution is the same as in Ref. [14]. In practice, it is simpler to implement the linear elasticity solution in a simulation: the
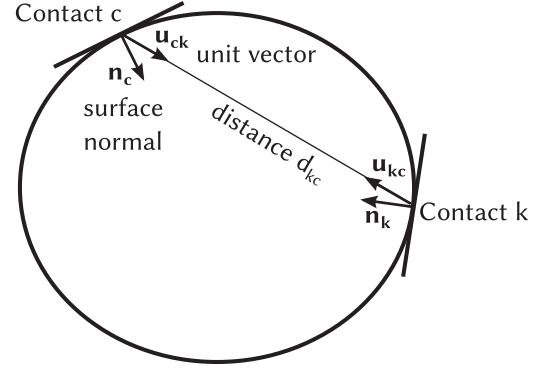

FIG. 2. Influence of one contact onto another. Contacts are not restricted to the surface of a sphere, their position is consistent with the grain deformations.

cross-contact influences are computed with Eq. (1), considering the current positions of contact points as in Fig. 2, without having to resort to a spherical approximation. However, in a dense packing, the grains do not form an infinite continuous half-space but rather a very complicated and everchanging boundary with pores between grains. For noncompressible materials (Poisson's ratio $\nu = 0.5$) the solution for an infinite full-space [17, 5.4.3] only induces a change in prefactor, $\gamma = 0.5$ instead of $\gamma = 1$ in Eq. (1). We therefore let γ be an adjustable parameter in order to account empirically for the geometry.

IV. MODELS

We consider the following models:

Independent contacts: The reference model with nondeformable overlapping spheres [2] and independent contacts with Hertz's law.

Point force on sphere: Bondareva's solution [15] for the deformations induced by a point force on a sphere. The radial component of Eqs. (7) and (8) in Ref. [15] is used for $\delta_{k \to c}$.

Sphere to sphere: The approximate solution by Gonzalez and Cuitiño [14] of a sphere-to-sphere contact [16]; $\delta_{k \to c}$ is then set to Eq. (3) in Ref. [14].

Elastic half-space: The above linear elasticity solution, Eq. (1), for the deformations induced by a point force on an infinite half-space, with $\gamma = 1$. As noted above, when $\nu = 0.5$, the only difference with the sphere-to-sphere solution is that contact points are applied at the location of the deformed grain surface, rather than being projected on a sphere.

MC-DEM: The full Eq. (1), adjusting γ so as to best match experimental measurements. We found a best fit at $\gamma \approx 1.19$ for the results presented below.

At each simulated time step, the total displacements $\sum_k \delta_{k \to c}$ are computed not only at the contact points, but also at the surface of each grain in the directions of the closest neighbors [Fig. 1(b)]. When these surface deformations are large enough that the particles would overlap, a new contact is created. That contact initially produces a zero force when the deformed surfaces barely touch. Hence, there is a null cross-contact influence according to Eq. (1), so the creation of new contacts is a continuous process. This method naturally handles the automatic creation of new contacts

due to particle deformations, which the basic DEM model is unable to achieve. With the same Young's modulus for each material in contact, the amount of deformation spreads equally in both particles [18]. Therefore, the contact position is geometrically defined as the average between the surface positions if they were overlapping. Unlike the standard DEM, where spheres are not deformable, the radius now effectively changes per contact. This yields geometric torques $f_t \times r$ due to nonsphericity, which are handled at no additional cost. In the standard DEM, only f_t varies with friction, while now r changes as well. However, recomputing the inertia matrix of each grain using the surface deformations would be very costly, so we keep the inertia of a sphere. With many contacts spread around the grain, we assume that the situation is isotropic enough that the sphere inertia is a reasonable approximation. Thus, only the $\delta_{k \to c}$ computations themselves significantly add to the simulation cost as $O(ZN)$, where Z is the number of contacts per grain and N the number of neighbors per grain.

V. EXPERIMENT

Our reference experiment consists of 514 hydrogel grains that are uniaxially compressed 20 times consecutively [8]. We have measured the system at each compression level, from strains of 0 to 13.4%. Each compression-unloading cycle comprises 50 full 3D scans where the top plate touches the grains, with 10 additional scans where the top plate is above the packing. We discard the first 5 compression cycles to let the system reach a reproducible configuration from cycle to cycle. We explicitly separate loading and unloading phases as some hysteresis is observed, which the simulations also reproduce. The full 3D force vectors are available experimentally at each contact [8]. In addition, we also measure the force exerted on the top plate at each scan. These statistics, averaged over all similar loading-unloading phases, form the "ground truth" that the DEM models must reproduce as accurately as possible.

The experimental particles are not completely spherical in their uncompressed state. In the simulations, we replace them by spheres with the same volume and same initial center of mass, and let the packing relax to a nearby state. This process yields a slight inflation of the simulated packing, which generates a nonzero force on the top plate in the least compressed samples, unlike the experiment. This effect is negligible in the most compressed states. We use our best estimate of the hydrogel Young's modulus $E = 23.3$ kPa. In order to match the quasistatic experimental regime with long-lasting contacts, we used a constant coefficient of restitution [19] close to one. That coefficient is not exactly one, however, since some dissipation is required on larger time scales to dissipate the top plate momentum and let the packing stabilize. We also use our best estimate of the intergrain coefficient of friction $\mu \approx 0.03$, although with an experimental error bar of ± 0.02. It is likely that friction between immersed hydrogel particles is not Coulombian. Nevertheless, and given its very low value, we assume in the DEM that friction is always saturated $F_t = \mu F_n$ with F_n given by the chosen model and F_t the magnitude of the tangential force component (whose direction opposes sliding). This is further justified by the fact that we discard the tangential terms in Eq. (1). For larger values of μ, with
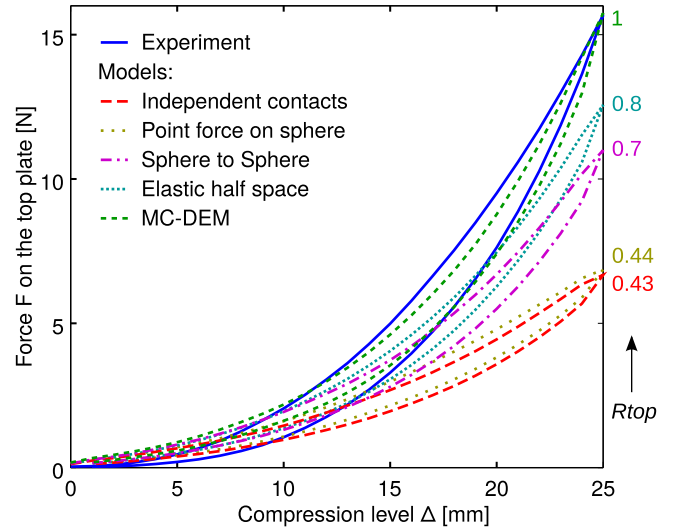

FIG. 3. (Color online) Force exerted on the top plate during a compression test, for the experimental data from [8] and all the simulation models mentioned above, for $\mu = 0.03$.

nonsaturated friction, it is possible to add contributions from other contacts to F_t with a similar formula [17].

The following metrics are defined to quantify the simulation accuracy and to assess the quality of each force model:

Rtop: The ratio between the force on the top plate computed in the simulation and the measured one, on average, at the maximum compression level. This value should be as close to one as possible. Figure 3 shows the top forces for the experimental data and the simulation models, at all compression levels. *Rtop* is shown on the right. The classic DEM model and the point force on sphere solutions are both off by more than 50%. The sphere-to-sphere and linear half-space models come closer, but the geometric correction by γ is necessary to reach a $Rtop = 1$.

errf: The root mean-squared (RMS) error for the force on the top plate at all compression levels. For simulations with *Rtop* close to 1, this measures the ability to also correctly reproduce the hysteresis between the compression and unloading phases visible in Fig. 3. None of the models is able to reproduce the experimental curve exactly, but the new MC-DEM model is the most accurate.

bhat: The above metrics only use the global measure of force exerted on the top plate from the experimental data, but we now have access to the full 3D forces at each contact. Due to the initial packing rearrangement, we can only compare statistical distributions, which the simulations must reproduce as closely as possible. One measure of closeness for distributions is the Bhattacharyya "distance," defined as $d = -\log B$ with $B = \int_0^\infty \sqrt{p(f)q(f)} df$, where p and q are the force distributions. This definition can consistently be averaged over all compression levels by using $D = -\log\langle B \rangle$. This is the measure we report as *bhat*, which is a global indicator of how closely the distributions in the simulation match the experimental ones. $D = 0$ would indicate a perfect match at all compression levels. The values in the least compression levels are biased by the initial packing rearrangement, but this
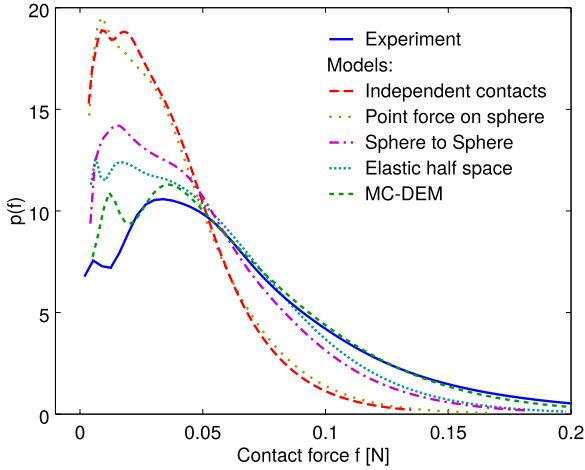
FIG. 4. (Color online) Comparison of the force distributions at intermediate compression $\Delta = 18$ mm during the unloading phase. This representative example is chosen to show values other than maximal compression. The *bhat* error measure in the main text captures all compression levels.

TABLE I. Metrics to compare DEM methods with experiment: Rtop: maximum compression force ratio at maximum compression; errf: root mean-squared error of the force response at all compression levels during compression and decompression; bhat: interparticle force probability distribution function match; errZ: RMSE of the contact number per particle; τ: weak force resolution.

Model	Rtop	errf	errZ	bhat $\times 10^2$	τ (mN)
Independent contacts	0.43	3.39	0.51	7.21	2.89
Point force on sphere	0.44	3.23	0.53	6.51	2.93
Sphere to sphere	0.70	1.82	0.34	2.57	3.35
Elastic Half Space	0.80	1.26	0.40	1.90	3.45
MC-DEM	1.00	0.41	0.26	0.98	4.00
Perfect fit	*1.00*	*0*	*0*	*0*	*<10*

is the same bias for all models. There is also an experimental lower resolution limit on weak forces that is not present in the simulations. Figure 4 shows distributions of $P(f)$ for the unloading phases, at compression level $\Delta = 18$ mm, where the force on the top plate is about half the maximum. As expected, the weak forces show the most discrepancy. Nevertheless, MC-DEM reproduces both the experimental distribution peak and the largest force values.

errZ: RMS error of the number of contacts per grain, after thresholding weak forces $f < \tau$ in the simulations and ignoring the corresponding contacts. The threshold τ that produces the best match and thus lowest RMS error for Z can

be used as an estimate for the experimental lowest resolution on the weakest forces. Here we find $\tau = 4$ mN, as shown in Table I. This is consistent with the average force in the least compression level reported in Ref. [8], $\langle f \rangle = 10$ mN. Figure 5 shows the number of contacts per grain after thresholding for all models. MC-DEM yields values closest to the experiment. When thresholding is not applied, simulation models produce $6.4 < Z < 6.5$ in the least compressed case: this is a side effect of the residual small compression, as uncompressed weakly frictional grains at rest are expected to produce values typically between 4 and 5 [20].

Table I summarizes all the configurations and their performances. The traditional DEM implementation with independent contacts clearly fails to reproduce the measurements. Implementing a linear spring model would make the match between numerics and experiments even less accurate, due to the lack of nonlinear stiffening at the contact level [1]. The solution for a point-force on a sphere boundary condition is not relevant in the case of multiple contacts and does
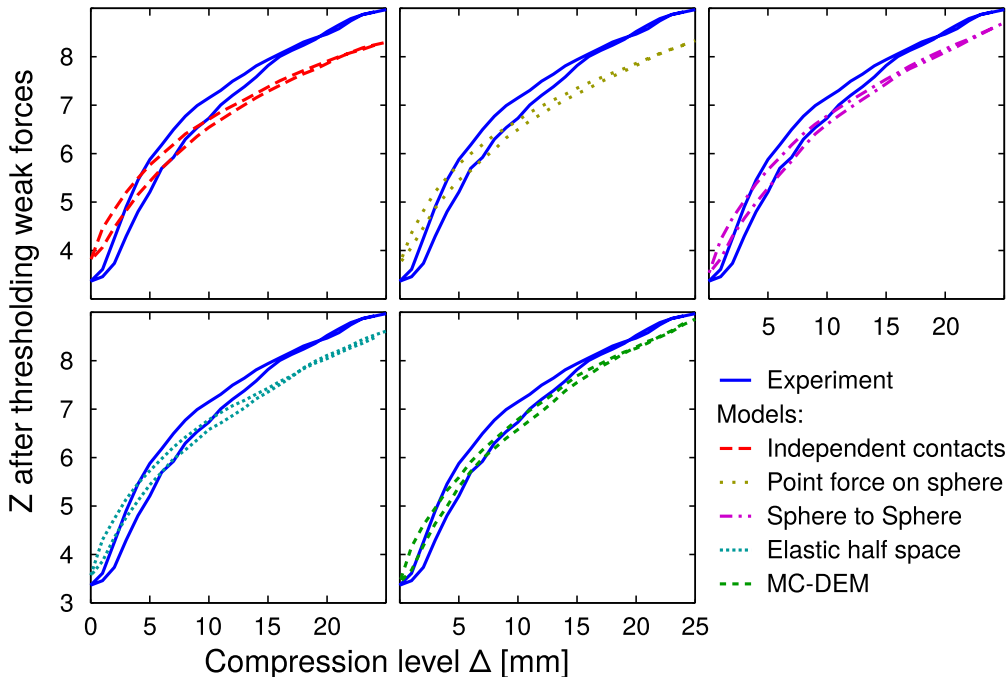

FIG. 5. (Color online) Number of contacts per grain Z after thresholding weak forces, averaged over multiple cycles.

not bring much improvement. The seminal multiple-contacts model proposed by Gonzalez and Cuitiño [14] offers good performance, but not as good as the half-space approximation from linear elasticity. Since these two models are equivalent when the contact positions are restricted to the surface of a sphere, this confirms that even slight surface deformations are important to accurately reproduce the experimental measures. MC-DEM, adjusting γ so that Rtop $= 1$, yields the best results on all quantifiers.

VI. MICROSCOPIC VARIABLE SCALING

In Ref. [8], we have established a new scaling law relating the macroscopic force on the top plate to microscopic quantities, which we validated with experimental data. We summarize the scaling law here briefly: a packing stress tensor can be computed [21] with a relation of the form $\sigma = 1/V \sum_{c \in V} \mathbf{b}_c \otimes \mathbf{f}_c$, with V an averaging volume and $c \in V$ the contacts in that volume. For each contact c, $\mathbf{b}_c$ is the vector between the centers of the grains and $\mathbf{f}_c$ is the force vector along the contact normal. Neglecting friction and nonsphericity, $\mathbf{b}_c$ and $\mathbf{f}_c$ are aligned; hence, the trace $\mathrm{tr}(\mathbf{b}_c \otimes \mathbf{f}_c) \propto \mathbf{b}_c \cdot \mathbf{f}_c$. The number of terms in the sum depends on the density of contacts, which is about $\frac{1}{2}Z\phi$, with Z the number of contacts per grain and ϕ the grain volume fraction within the packing. With density matching, we can neglect hydrostatic pressure gradients, and due to sphericity, we can set the pressure on the top plate $P \propto \mathbf{b}_c \cdot \mathbf{f}_c$. Hence, with F, f and averaging performed as explained in Fig. 6:

$$F \propto P \propto \langle Z \rangle \langle \phi \rangle \langle |\mathbf{b}| \rangle \langle |\mathbf{f}| \rangle. \tag{2}$$
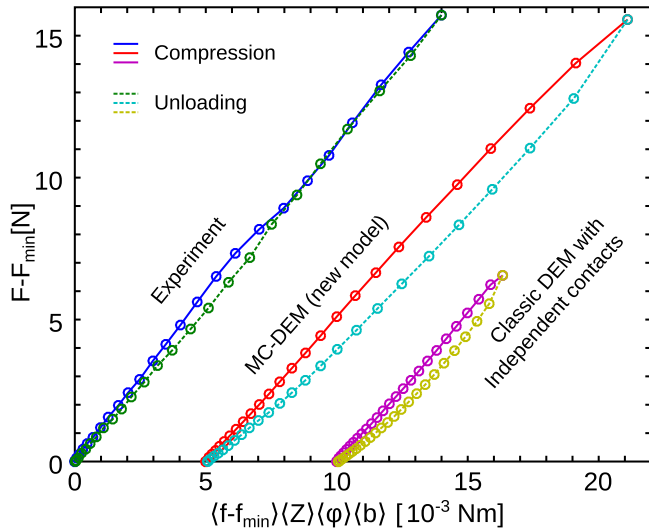
FIG. 6. (Color online) Validation that the scaling law from Ref. [8], derived from experimental data, also holds in the simulation. Here, F is the force exerted by the grains on the top plate, f is the average force at each contact, Z is the number of contacts per grain, φ is the volume fraction within the packing (starting one diameter away from walls), and b is the distance between grain centers. Microscopic quantities were averaged on all grains and contacts within the packing. Data was then averaged on the 15 retained compression or unloading phases with the same strain. Each marker in the diagram represents one such strain level. MC-DEM and the usual DEM data have been shifted for clarity by 5 and 10 mNm, respectively.

The ability of the simulations to reproduce this scaling law is a requirement for a quantitative match with experiments. In Fig. 6 we show both the experimental data, the result for MC-DEM and the result for the classic, independent contacts, DEM simulation. The new model presents an overall good agreement with the experiment data. Differences are a slightly lower coefficient of proportionality between the top force and the microscopic quantities, as well as more hysteresis between the compression and unloading phases. The maximum top force F for both models matches the Rtop data given in Table I, with a very small $F_{\min}$ offset. Irrespective of F, the scaling for the simulations presents some curvature in the unloading phase, which does not show up in the experimental data (with less relative curvature for MC-DEM). One possible explanation for the discrepancy could be friction, which is assumed to follow Coulomb's law in these simulations, while this is not necessarily valid for the hydrogel particles used in the experiment. Remarkably, the slope is nearly the same in all three cases, despite the top force being halved for the same compression level in the classic DEM case. This suggests that the mean-field scaling relation that we derived in Ref. [8] is quite robust to model variations, and sensitive only to the values of F and the microscopic quantities, independent of the model by which these were produced.

VII. DISCUSSION

The new model, which we introduce here, clearly shows that current DEM techniques can be much improved by taking into account correlations between multiple contacts, at least when simulating dense packings. We have introduced a simple and effective way to compensate for the geometry of the boundary conditions within the packing, in the form of an empirical prefactor γ for the cross-contact influences. Ideally, γ should be replaced by a correct accounting for the boundary conditions within the packing, but this is very complicated and any solution would need to be updated at every simulation step. Working at the grain level and recoupling the force propagation through the contact law seems the only practicable approach for DEM. Thus, replacing the complex boundaries within the packing with a functional dependency on statistics at the grain level [22] would be an interesting option for building better models. Future models also need to account for lower Poisson's ratios $\nu < 0.5$. In the particular case of $\nu = 0$, no correlation should be introduced between orthogonal contacts. Yet both the linear elasticity half-space solution [Ref. [17] and Eq. (1)], as well as the sphere-to-sphere contact approximation [14], predict some cross-contact displacements $\delta_{k \to c}$ in this situation.

VIII. CONCLUSION

We have shown that our multiple-contact implementation in DEM captures the force dynamics of a compressed sphere packings very well, both at the macroscopic and microscopic level, including the full distribution of forces in 3D. Our approach performs significantly better than current DEM techniques [1], where contacts are considered independently, but also better than some other approaches to implementations of multiple contact modeling. We have introduced a simple and

effective way to compensate for the geometry of the boundary conditions within the packing, in the form of an empirical prefactor γ. MC-DEM is thus an effective way to introduce the multiple-contacts correlation idea (similar to Ref. [14]) in the context of DEM. Part of the goal here is to raise awareness on this issue and to show that, at least in our case, these correlations are necessary. The full extent of the validity of this model is, however, an open question. In particular, we have only compared our simulations to experiments on soft particles. Although Eq. (1) does not depend on the Young's modulus, which appears both in the force in the numerator and in the denominator, it may be that MC-DEM becomes less relevant with harder materials, except perhaps close to jamming, where a proper accounting for the creation of new contacts is likely to matter most. Similarly, diluted flows and granular gases with binary collisions would not benefit from the multiple-contact correlations. Perhaps more importantly,

the empirical parameter γ in Eq. (1) may itself depend on other microstructural parameters, like the number of contacts per grain Z and the packing fraction ϕ, which are likely to affect the quality of the elastic half-space approximation. We thus hope that our work, showing that multiple contacts correlations must be taken into account at least in the reference case we present, will induce additional new MC-DEM model variants for more complicated situations, ultimately providing better quantitative predictions of granular material behaviors.

ACKNOWLEDGMENTS

[1] S. Luding, Introduction to discrete element methods: Basics of contact force models and how to perform the micro-macro transition to continuum theory, Eur. J. Env. Civil Eng. **12**, 785 (2008).

[2] P. A. Cundall and O. D. L. Strack, A discrete numerical model for granular assemblies, Geotechnique **29**, 47 (1979).

[3] J. Brujić, S. F. Edwards, D. V. Grinev, I. Hopkinson, D. Brujić, and H. A. Makse, 3D bulk measurements of the force distribution in a compressed emulsion system, Faraday Discuss. **123**, 207 (2003).

[4] J. Zhou, S. Long, Q. Wang, and A. D. Dinsmore, Measurement of forces inside a three-dimensional pile of frictionless droplets, Science **312**, 1631 (2006).

[5] J. E. Andrade and C. F. Avila, Granular element method (GEM): linking interparticle forces with macroscopic loading, Granular Matter **14**, 51 (2012).

[6] M. Saadatfar *et al.*, Mapping forces in a 3D elastic assembly of grains, J. Mech. Phys. Solids **60**, 55 (2012).

[7] J. A. Dijksman, H. Zheng, and R. P. Behringer, Imaging soft sphere packings in a novel triaxial shear setup, in *Powders and Grains 2013*, Proceedings of the 7th International Conference on Micromechanics of Granular Media, Sydney, Australia, edited by A. Yu, K. Dong, R. Yang, and S. Luding, AIP Conference Proceedings Vol. 1542 (AIP, Melville, New York, 2013), pp. 457–460.

[8] N. Brodu, J. A. Dijksman, and R. P. Behringer, Spanning the scales of granular materials through microscopic force imaging, Nat. Commun. **6**, 6361 (2015).

[9] H. M. Princen and A. D. Kiss, Rheology of foams and highly concentrated emulsions: III. Static shear modulus, J. Colloid Interface Sci. **112**, 427 (1986).

[10] J. T. Jenkins and E. Askari, Hydraulic theory for a debris flow supported on a collisional shear layer, Chaos **9**, 654 (1999).

[11] N. Brodu, R. Delannay, A. Valance, and P. Richard, New patterns in high-speed granular flows, J. Fluid Mech. (to be published), arXiv:1210.7478.

[12] A. H. Clark, L. Kondic, and R. P. Behringer, Particle scale dynamics in granular impact, Phys. Rev. Lett. **109**, 238302 (2012).

[13] A. H. Clark, A. J. Petersen, L. Kondic, and R. P. Behringer, Nonlinear sound during granular impact, arXiv:1408.1971.

[14] M. Gonzalez and A. Cuitino, A nonlocal contact formulation for confined granular systems, J. Mech. Phys. Solids **60**, 333 (2012).

[15] V. F. Bondareva, On the effect of an axisymmetric normal loading on an elastic sphere, J. Appl. Math. Mech. **33**, 1001 (1969).

[16] O. Zhupanska, Contact problem for elastic spheres: Applicability of the Hertz theory to non-small contact areas, Int. J. Eng. Sci. **49**, 576 (2011).

[17] A. Bower, *Applied Mechanics of Solids* (CRC Press, Boca Raton, 2010).

[18] L. D. Landau and E. M. Lifshitz, *Theory of Elasticity, Vol. 7 of A Course of Theoretical Physics* (Pergamon Press, Oxford, 1970).

[19] Y. Tsuji, T. Tanaka, and T. Ishida, Lagrangian numerical simulation of plug flow of cohesionless particles in a horizontal pipe, Powder Technol. **71**, 239 (1992).

[20] L. E. Silbert, D. Ertaş, G. S. Grest, T. C. Halsey, and D. Levine, Geometry of frictionless and frictional sphere packings, Phys. Rev. E **65**, 031304 (2002).

[21] M. Babic, Average balance equations for granular materials, Int. J. Eng. Sci. **35**, 523 (1997).

[22] M. Clusel, E. Corwin, A. O. N. Siemens, and J. Brujić, A "granocentric" model for random packing of jammed emulsions, Nature **460**, 611 (2009).

[23] N. Brodu, Source code for the MC-DEM simulations, available for download at http://nicolas.brodu.net/code/dymo/, released under GNU LGPL v2 or more recent.